NANO LETTERS

pubs.acs.org/NanoLett

Subwavelength Plasmonic Lasing from a Semiconductor Nanodisk with Silver Nanopan Cavity

Soon-Hong Kwon,[†] Ju-Hyung Kang,[‡] Christian Seassal,[§] Sun-Kyung Kim,[†] Philippe Regreny,[§] Yong-Hee Lee,[‡] Charles M. Lieber,*[,∥,⊥] and Hong-Gyu Park*[,†]

[†]Department of Physics, Korea University, Seoul 136-701, Korea, [‡]Department of Physics, KAIST, Daejeon 305-701, Korea, [§]Université de Lyon, Institut des Nanotechnologies de Lyon INL-UMR 5270, CNRS, Ecole Centrale de Lyon, 36 Avenue Guy de Collongue, F-69134 Ecully Cedex, France, [∥]Department of Chemistry and Chemical Biology, Harvard University, Cambridge, Massachusetts 02138, and [⊥]School of Engineering and Applied Sciences, Harvard University, Cambridge, Massachusetts 02138

ABSTRACT We report the experimental demonstration of an optically pumped silver-nanopan plasmonic laser with a subwavelength mode volume of $0.56(\lambda/2n)^3$. The lasing mode is clearly identified as a whispering-gallery plasmonic mode confined at the bottom of the silver nanopan from measurements of the spectrum, mode image, and polarization state, as well as agreement with numerical simulations. In addition, the significant temperature-dependent lasing threshold of the plasmonic mode contrasts and distinguishes them from optical modes. Our demonstration and understanding of these subwavelength plasmonic lasers represent a significant step toward faster, smaller coherent light sources.

KEYWORDS Surface plasmons, active plasmonics, nanolasers, subwavelength mode volumes

Investigations of ultrasmall light sources have opened up the possibilities of demonstrating low-threshold lasers,[1] efficient single photon sources,[2] and ultrafast modulation sources[3] as well as studying strong light−matter interactions.[4,5] Wavelength-scale lasers with mode volumes approaching a cubic half-wavelength in material, $(\lambda/2n)^3$, have been demonstrated in dielectric cavities such as photonic crystals[6] and semiconductor nanowires.[7,8] In addition, lasers operating with optical modes excited in metal-clad cavities[1,9,10] showed mode volumes slightly smaller than $(\lambda/2n)^3$. More recently, plasmonic cavities capable of reducing mode volumes below the diffraction limit of conventional optics have been proposed,[11−16] and reports have successfully demonstrated lasing in several structures.[17−19] However, most plasmonic cavities still show wavelength-scale or marginally subwavelength-scale mode volumes,[13,17,18] and thus the full three-dimensional (3D) confinement of surface plasmons in a subwavelength volume remains a challenge. Furthermore, plasmonic and optical modes have been simultaneously excited in such wavelength-scale cavities,[13,17] making it difficult to identify clearly observed resonant modes as plasmonic versus optical. To address these issues and demonstrate unambiguously subwavelength plasmonic lasers, we have designed and characterized the optical properties and temperature-dependent lasing thresholds of semiconductor nanodisks with 3D confinement imposed by a silver-nanopan cavity.

Our plasmonic laser structure consists of a 235 nm thick InP disk with four InAsP quantum wells (QWs) in the middle

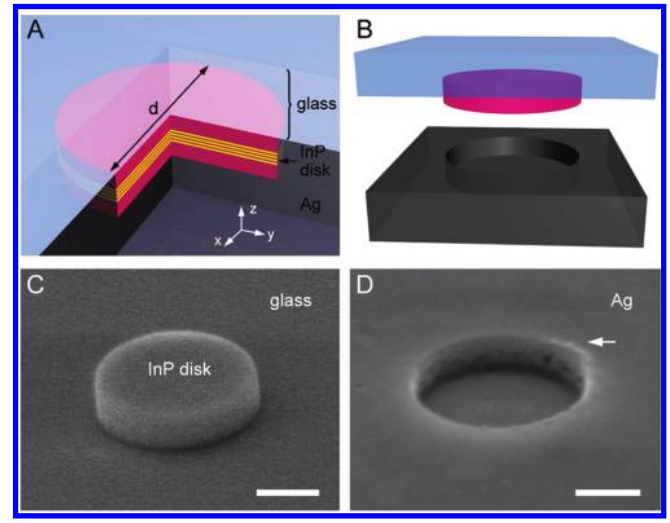

FIGURE 1. Structure of the plasmonic nanopan cavity. (A) Schematic diagram of the nanodisk/nanopan structure. The top of the InP disk was bonded to a transparent glass substrate, and the bottom and sidewall of the disk were coated with silver. Four InAsP QWs were embedded in the middle of the disk. *d* is the diameter of the disk. (B) Schematic diagram of the removal of the silver nanopan. The blue, magenta, and gray colors correspond to the glass, InP disk, and silver, respectively. (C) SEM image of the InP disk on glass prior to silver deposition. (D) SEM image of the silver film separated from the disk. The white arrow indicates damage by the separation process. Scale bars in C and D are 400 nm.

* Corresponding authors, cml@cmliris.harvard.edu and hgpark@korea.ac.kr.
Received for review: 06/20/2010
Published on Web: 08/12/2010

DOI: 10.1021/nl1021706 | *Nano Lett.* **2010,** *10,* 3679–3683

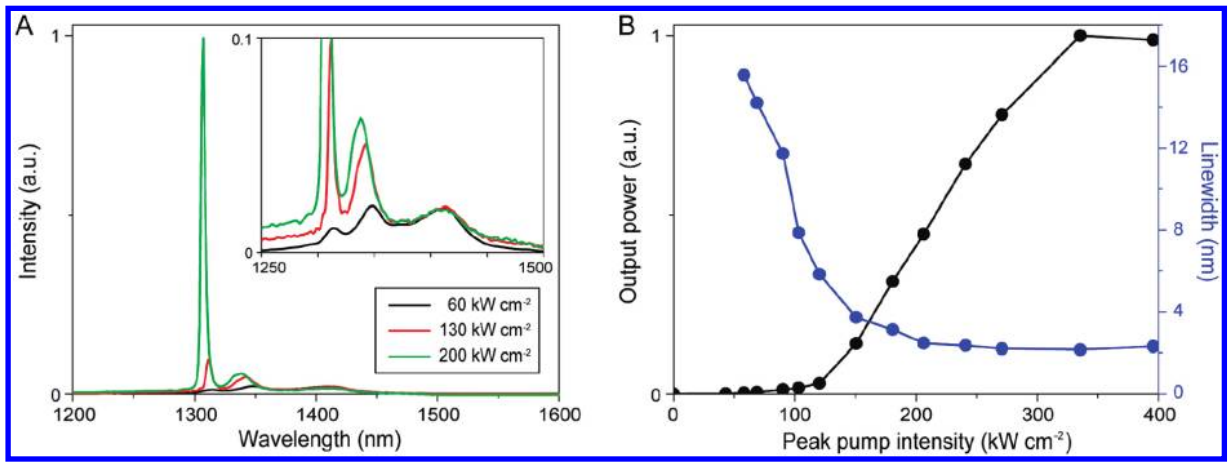

FIGURE 2. Plasmonic lasing in the nanodisk/nanopan structure. (A) Measured spectra at the absorbed peak pump intensities of 60 (black), 130 (red), and 200 kW cm^{-2} (green) at 8 K for d = 1000 nm structure. The inset shows the magnification of the spectra in the range of wavelengths including the lasing peak at 1308 nm, nonlasing side peak at 1338 nm, and QW emission at 1420 nm. (B) Output power (black) and linewidth (blue) of the plasmonic laser were measured as a function of the absorbed peak pump intensity. Data were recorded as described in Methods in the Supporting Information.

of the disk as an active medium and a cavity structure consisting of a silver nanopan as shown in panels A and B of Figure 1. The top of the disk is bonded to a transparent glass substrate[20] that allows efficient optical pumping and photoluminescence (PL) collection. The bottom and sidewall of the disk are covered with silver to construct the nanopan cavity, where the semiconductor-filled silver nanopan structure is expected to generate plasmonic modes. To fabricate the semiconductor/cavity structure, InP disks were formed on the glass substrate using an electron-beam lithography and dry etching process (Figure 1C), and silver was then deposited on the disks (Methods in Supporting Information). Panels C and D of Figure 1 show representative scanning electron microscopy (SEM) images of an InP disk and silver nanopan, respectively, after the silver was "peeled off" from the disk as presented schematically in Figure 1B. The measured roughness of the bottom surface of the silver nanopan (rms = 0.59 nm) is similar to that of the epitaxial InP disk surface (rms = 0.22 nm).[21] Because a smooth metal surface is essential for reducing the scattering loss and increasing the plasmonic propagation length,[21−23] the 0.59 nm smooth lower surface of the silver is expected to support high-quality (Q) plasmonic modes at the bottom of the nanopan. We do note that the sidewall surface was rougher owing to damage during dry etching process used to fabricate the InP nanodisk and could reduce the overall efficiency of the cavity.

To assess initially the characteristics of the nanodisk/nanopan structures, we optically pumped the InP using a 980 nm pulsed laser diode at 8 K (see Methods in Supporting Information). In a disk/nanopan structure with d = 1000 nm (Figure 2), a PL spectrum from the InAsP QWs with peak at 1420 nm[24] was observed at pump intensities below 40 kW cm^{-2}. At moderate pump intensities (40−120 kW cm^{-2}), two new peaks appear at 1308 and 1338 nm (Figure 2A). Similar closely spaced peaks with ≤30 nm peak-to-peak separation were in PL measurements on disk/nanopan structures with d = 900−1200 nm (Figure S3, Supporting Information). We discuss the origin of these two peaks below in conjunction with numerical simulations. In addition, as the pump intensity increased, the shorter wavelength peak of 1308 nm became dominant with rapid increase in intensity and decrease in full width at half-maximum (fwhm) linewidth, while the peak at 1338 nm and longer wavelength QW emission at 1420 nm appeared to saturate, suggestive that lasing is achieved in the 1308 nm peak.

To assess clearly potential lasing in the 1308 nm mode, we measured the output power as a function of the absorbed peak pump intensity (black, Figure 2B). In this plot, the nonlinear response of the output power is clearly observed with a lasing threshold of ∼120 kW cm^{-2}. Analysis of the linewidth as a function of pump intensity further showed an abrupt decrease to a constant value soon after the changeover to superlinear behavior of the output power (blue, Figure 2B).[16,25] These observations and saturation of the 1338 nm and QW at 1420 nm emission peaks (inset, Figure 2A)[1] are all consistent with lasing in the disk/nanopan structure. We also note similar characteristics consistent with lasing were measured in a disk/nanopan structure with d = 1250 nm (Figure S1, Supporting Information).

To further examine the lasing modes, we measured the mode images and polarization states. In the disk/nanopan structure with d = 1000 nm, the lasing mode profile captured by an infrared (IR) camera has circular symmetry with an intensity node at the center (left, Figure 3A). The polarization-resolved mode profiles were also captured after placing a linear polarizer in front of the camera (middle and right, Figure 3A), and the images with an intensity minimum along the polarizer axis were observed. Together with these images, the output power measured as a function of the polarization angle, using a linear polarizer in front of the spectrometer (Methods in Supporting Information), also

DOI: 10.1021/nl1021706 | Nano Lett. 2010, 10, 3679–3683

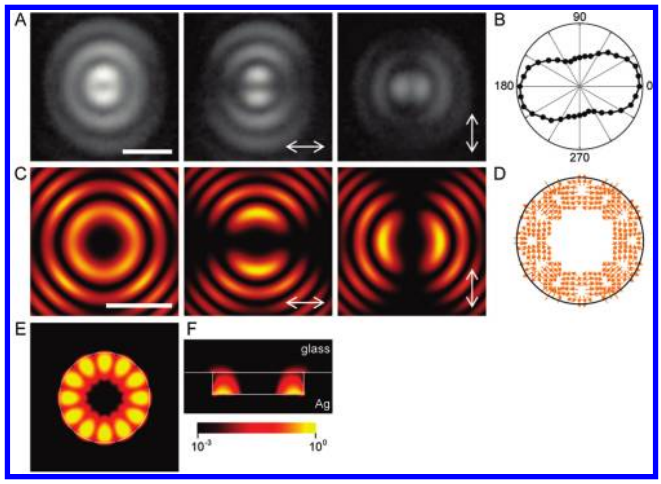

FIGURE 3. The mode image and polarization state of the plasmonic laser. (A) The lasing mode image captured by an IR camera without a polarizer (left) for a d = 1000 nm structure. The polarization-resolved images were also captured using horizontal (middle) and vertical polarization (right). The scale bar is 4 μm. (B) The measured output power of the lasing mode as a function of the polarization angle, using a linear polarizer placed in front of the spectrometer. (C) The calculated z-component of the Poynting vector of the WG plasmonic mode of Figure 3E (left). The z-components of the horizontally and vertically polarized Poynting vector are shown in the middle and right panels, respectively. The calculation was performed at a position 5 μm above the InP disk. The scale bar is 2 μm. (D) The calculated electric field directions of the WG plasmonic mode in panel E. (E, F) The calculated electric field intensity (log E^2) profiles of the WG plasmonic mode confined at the bottom of the nanopan. The electric field directions (D) and the top view of the field profile (E) were calculated at the bottom silver surface in the side view (F).

shows the polarization state of the mode.[6] No preferred direction of polarization was observed from the top of the disk/nanopan structure (Figure 3B).

3D finite-difference time-domain (FDTD) simulations were performed to identify the lasing modes (see Methods in Supporting Information). Among the resonant modes excited in the disk/nanopan structure with d = 1000 nm, we investigated the whispering-gallery (WG) plasmonic mode confined at the bottom of the disk/nanopan interface (Figure 3, panels C–F). To compare FDTD simulations of the WG plasmonic mode with the experimental results shown in Figure 3A, we calculated the z-component of the Poynting vector and the polarized Poynting vectors with horizontal and vertical electric field components at a position 5 μm above the InP disk (Figure 3C). Notably, the calculated Poynting vectors agree well with the measured mode images of Figure 3A. In addition, the electric field directions of this WG plasmonic mode were calculated to be symmetrically distributed at the bottom surface of the nanopan (Figure 3D), which is consistent with the absence of a preferred direction in the experimentally measured polarization state data shown in Figure 3B. Taken together these simulation results strongly support a conclusion that the observed lasing arises from a WG plasmonic mode.

Our FDTD simulations also show that the WG plasmonic mode is strongly confined at the bottom of disk/nanopan interface. Specifically, the top and side views of the near-field mode profiles associated with the WG plasmonic mode (Figure 3, panels E and F) demonstrate strong symmetrical confinement at the bottom edge of the disk/nanopan. Significantly, the mode volume calculated for this WG plasmonic mode is 0.003 μm^3 or 0.56 $(\lambda/2n)^3$, which is substantially smaller than previously reported mode volumes for dielectric optical cavities[6−8] and comparable to those for metal-clad optical cavities,[1,10] showing the full 3D confinement of surface plasmons in a subwavelength volume.

Further FDTD analysis enables us to elucidate other details of the experimental results. First, it is noted that two types of WG optical modes with electric fields normal and parallel to the plane of an InP disk are excited without a silver nanopan.[26] Since electric fields of a plasmonic mode are perpendicular to the metal surfaces,[22,23] introduction of the silver nanopan can lead to effective conversion of the WG optical modes into plasmonic modes. Given this suggestion, there will be two types of WG plasmonic modes, where one is defined at the bottom of the nanopan and the other is at the sidewall, which are confirmed by our FDTD simulations. The WG plasmonic mode defined at the bottom has an intensity minimum along the polarization axis in the calculated Poynting vector while the mode at the sidewall has an intensity maximum. The measured polarization-resolved mode images of Figure 3A can thus identify the lasing mode as the WG plasmonic mode excited at the bottom of the silver nanopan. In addition, by comparing the calculated and measured wavelengths, we note that the two peaks observed in Figure 2A are the resonant peaks of broken degeneracy in the doubly degenerate WG plasmonic modes. We suggest that the relatively large splitting of these degenerate modes is due to scattering induced by the higher surface roughness[26,27] of the InP/silver sidewall versus bottom (Figure 1D), although future studies will be necessary to prove the point.

To further investigate a difference in optical characteristics between the plasmonic and optical lasing modes, the temperature dependence of the threshold was measured (Figure 4). In the light-in versus light-out curves measured in the plasmonic laser of Figure 2, the threshold increased with temperature from 8 to 80 K and no lasing was observed at 300 K (Figure 4A). Similar temperature-dependent lasing threshold results were obtained in the plasmonic mode in a disk/nanopan structure with d = 1250 nm (Figure S1F, Supporting Information). On the other hand, the thresholds of the optical lasing mode observed in the disk/nanopan structure with d = 700 nm (Figure S2, Supporting Information) remained almost constant from 8 to 300 K as shown in Figure 4B. The lasing thresholds of both plasmonic and optical modes were plotted as a function of temperature for comparison in Figure 4C. The threshold of the plasmonic

DOI: 10.1021/nl1021706 | *Nano Lett.* **2010,** *10,* 3679–3683

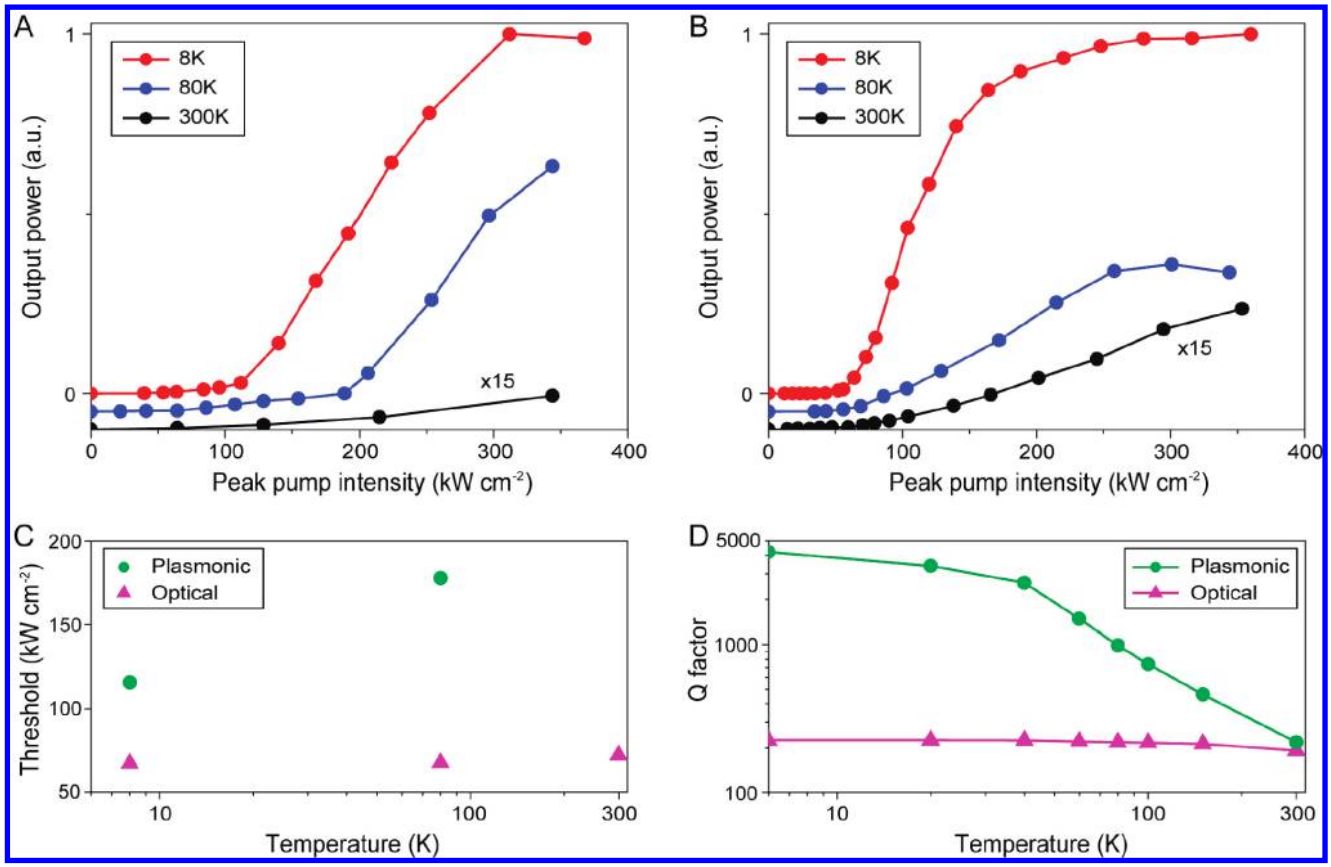

FIGURE 4. Temperature dependence of lasing threshold. (A) Light-in versus light-out curves measured in the plasmonic laser of Figure 2 at 1308 nm at 8 (red), 80 (blue), and 300 K (black). No lasing was observed at 300 K. (B) Light-in versus light-out curves measured in the optical-mode laser at 1251 nm (Figure S2) at 8 (red), 80 (blue), and 300 K (black). The curves in A and B are offset for clarity. (C) The measured lasing thresholds of the plasmonic and optical modes were plotted as a function of temperature. Points are from data in A and B. (D) Calculated *Q* factors of the plasmonic and optical modes as a function of temperature. The PL measurements and FDTD simulations for *Q* factors were performed as described in the Methods in Supporting Information.

lasing mode depends sensitively on the temperature, and this temperature dependence distinguishes them from optical modes.

Q factors of the plasmonic and optical modes were also calculated as a function of temperature by the FDTD method (Figure 4D).[28] The *Q* factor of the plasmonic mode decreases considerably with increasing temperature while the *Q* factor of the optical mode is independent of temperature. This simulation is consistent with the fact that metal absorption increases rapidly in plasmonic modes with increasing temperature for modes having an intensity maximum at the dielectric−metal interface, whereas an optical mode with an intensity minimum at the interface shows small change with temperature.[1,14,29−31] In addition, the FDTD results strongly support the experimental measurements in which the plasmonic and optical lasing modes show a distinguishable temperature dependence of the threshold. The optical loss plays a critical role in determining the threshold dependence in the disk/nanopan structure, where the resonant wavelength and pumping conditions of the plasmonic lasing are similar to those of the optical mode at each temperature. Therefore, measurements of the lasing threshold at different temperatures can provide a useful method for examining and distinguishing plasmonic versus optical lasing modes in metallic cavity structures.

Finally, to understand clearly the effect of metal in the disk/nanopan structure on optical modes, InP disks without silver nanopan cavity were optically pumped at 8 K (Figure S4, Supporting Information). Interestingly, lasing with conventional optical WG mode was observed only in the disks with a diameter of ≥1500 nm. In particular, the linearly polarized optical mode shown in Figure S2 was not observed in the InP disk with the same diameter of 700 nm due to severe optical loss into the glass substrate. This control experiment demonstrates that a metal coating on a dielectric cavity can have a significant effect on the properties of optical modes, such as optical loss and lasing threshold, and can lead to the excitation of distinct optical modes.[9] Hence, to distinguish clearly plasmonic and optical modes, it can be useful to investigate the properties of optical modes without the cavity structure. However, use of distinct temperature dependence of the plasmonic and optical thresholds can be exploited effectively for understanding plasmonic structures where removal of the cavity may be impractical.

In summary, we successfully demonstrated subwavelength plasmonic nanopan lasers for the first time. The lasing

DOI: 10.1021/nl1021706 | *Nano Lett.* **2010,** *10,* 3679–3683

mode was identified unambiguously as a WG plasmonic mode confined at the bottom of the nanopan/InP disk interface from measurements of the lasing spectrum, mode image, polarization state, and significant temperature-dependent threshold. This plasmonic mode has a subwavelength mode volume of $0.56(\lambda/2n)^3$, which is smaller than the lower limit of an optical cavity. Our progress in demonstrating a subwavelength semiconductor nanodisk/nanopan plasmonic laser represents an important step toward further miniaturization of coherent light sources as well as fast all-optical processing in an ultracompact photonic integrated circuit.[32]

Acknowledgment. We thank Emmanuel Augendre and Lea Di Cioccio, CEA-LETI, for support on wafer bonding. H.G.P. acknowledges support of this work by Creative Research Initiatives (2009-0081565) of MEST/KOSEF. C.M.L. acknowledges support of this work by the Air Force Office of Scientific Research. Y.H.L. acknowledges support of this work by a KICOS grant (M6060500007-06A0500-00710). C.S. acknowledges support of this work by the French–Korean LIA.

Supporting Information Available. Detailed descriptions of fabrication, measurement, and FDTD simulation and four additional figures. This material is available free of charge via the Internet at http://pubs.acs.org.

REFERENCES AND NOTES

(1) Hill, M. T.; Oei, Y.-S.; Smalbrugge, B.; Zhu, Y.; Vries, T. D.; Veldhoven, P. J. V.; Otten, F. W. M. V.; Eijkemans, T. J.; Turkiewicz, J. P.; Waardt, H. D.; Geluk, E. J.; Kwon, S.-H.; Lee, Y.-H.; Notzel, R.; Smit, M. K. *Nat. Photonics* **2007**, *1*, 589–594.
(2) Akimov, A. V.; Mukherjee, A.; Yu, C. L.; Chang, D. E.; Zibrov, A. S.; Hemmer, P. R.; Park, H.; Lukin, M. D. *Nature* **2007**, *450*, 402–406.
(3) Altug, H.; Englund, D.; Vuckovic, J. *Nat. Phys.* **2006**, *2*, 484–488.
(4) Chang, D. E.; Sorensen, A. S.; Hemmer, P. R.; Lukin, M. D. *Phys. Rev. Lett.* **2006**, *97*, No. 053002.
(5) Vahala, K. J. *Nature* **2003**, *424*, 839–846.
(6) Park, H.-G.; Kim, S.-H.; Kwon, S.-H.; Ju, Y.-G.; Yang, J.-K.; Baek, J.-H.; Kim, S.-B.; Lee, Y.-H. *Science* **2004**, *305*, 1444–1447.
(7) Huang, M. H.; Mao, S.; Feick, H.; Yan, H.; Wu, Y.; Kind, H.; Weber, E.; Russo, R.; Yang, P. *Science* **2001**, *292*, 1897–1899.
(8) Duan, X.; Huang, Y.; Agarwal, R.; Lieber, C. M. *Nature* **2003**, *421*, 241–245.
(9) Nezhad, M. P.; Simic, A.; Bondarenko, O.; Slutsky, B.; Mizrahi, A.; Feng, L.; Lomakin, V.; Fainman, Y. *Nat. Photonics* **2010**, *4*, 395–399.
(10) Yu, K.; Lakhani, A.; Wu, M. C. *Opt. Express* **2010**, *18*, 8790–8799.
(11) Miyazaki, H. T.; Kurokawa, Y. *Phys. Rev. Lett.* **2006**, *96*, No. 097401.
(12) Sorger, V. J.; Oulton, R. F.; Yao, J.; Bartal, G.; Zhang, X. *Nano Lett.* **2009**, *9*, 3489–3493.
(13) Min, B.; Ostby, E.; Sorger, V.; Ulin-Avila, E.; Yang, L.; Zhang, X.; Vahala, K. *Nature* **2009**, *457*, 455–458.
(14) Seo, M.-K.; Kwon, S.-H.; Ee, H.-S.; Park, H.-G. *Nano Lett.* **2009**, *9*, 4078–4082.
(15) Bergman, D. J.; Stockman, M. I. *Phys. Rev. Lett.* **2003**, *90*, No. 027402.
(16) Stockman, M. I. *J. Opt.* **2010**, *12*, No. 024004.
(17) Oulton, R. F.; Sorger, V. J.; Zentgraf, T.; Ma, R.-M.; Gladden, C.; Dai, L.; Bartal, G.; Zhang, X. *Nature* **2009**, *461*, 629–632.
(18) Hill, M. T.; Marell, M.; Leong, E. S. P.; Smalbrugge, B.; Zhu, Y.; Sun, M.; Veldhoven, P. J.; Geluk, E. J.; Karouta, F.; Oei, Y.-S.; Nötzel, R.; Ning, C.-Z.; Smit, M. K. *Opt. Express* **2009**, *17*, 11107–11112.
(19) Noginov, M. A.; Zhu, G.; Belgrave, A. M.; Bakker, R.; Shalaev, V. M.; Narimanov, E. E.; Stout, S.; Herz, E.; Suteewong, T.; Wiesner, U. *Nature* **2009**, *460*, 1110–1112.
(20) Martínez, L. J.; Alén, B.; Prieto, I.; Galisteo-López, J. F.; Galli, M.; Andreani, L. C.; Seassal, C.; Viktorovitch, P.; Postigo, P. A. *Opt. Express* **2009**, *17*, 15043–15051.
(21) Nagpal, P.; Lindquist, N. C.; Oh, S.-H.; Norris, D. J. *Science* **2009**, *325*, 594–597.
(22) Maier, S. A. *Plasmonics: Fundamentals and Applications*; Springer: Berlin, 2007.
(23) *Surface Plasmon Nanophotonics*; Brongersma, M. L., Kik, P. G., Eds.; Springer: Berlin, 2007.
(24) Lee, C.-Y.; Shiao, H.-P.; Wu, M.-C.; Chen, C.-W. *J. Vac. Sci. Technol., B* **1999**, *17*, 2530–2535.
(25) Mohideen, U.; Slusher, R. E.; Jahnke, F.; Koch, S. W. *Phys. Rev. Lett.* **1994**, *73*, 1785–1788.
(26) Borselli, M.; Srinivasan, K.; Barclay, P. E.; Painter, O. *Appl. Phys. Lett.* **2004**, *85*, 3693–3695.
(27) Zhu, J.; Ozdemir, S. K.; Xiao, Y.-F.; Li, L.; He, L.; Chen, D.-R.; Yang, L. *Nat. Photonics* **2010**, *4*, 46–49.
(28) The *Q* factor of the plasmonic mode is estimated to be ≤350 from the below-threshold linewidth in Figure 2, while the calculated *Q* factor is >3500 in Figure 4D.
(29) Gong, Y. Y.; Vuckovic, J. *Appl. Phys. Lett.* **2007**, *90*, No. 033113.
(30) Mayy, M.; Zhu, G.; Mayy, E.; Yakim, A.; Webb, A.; Livenere, J.; Li, H.; Bobb, D.; Noginov, M. A. Conference on Lasers and Electro-Optics/International Quantum Electronics Conference, 2009.
(31) In contrast to ref 30, our experimental results agree well with the previously reported results (refs 1, 14, and 29).
(32) Polman, A. *Science* **2008**, *322*, 868–869.

DOI: 10.1021/nl1021706 | *Nano Lett.* **2010,** *10,* 3679–-3683